Click-Chemistry Hydrogel Delivery Aggregation-Induced Emission-Active Nanovesicles Enables "One-Stop" Remodeling and Antibiosis on Deep Scald Wound

Xu Chen[1], Meijiao Zhao[2], Qihu Xie[3], Sitong Zhou[4], Yanan Qianzuo[2], Xiaoping Zhong[3], Judun Zheng[2], Ronghua Yang[5], Xianjin Du[6], Jinyu Xia[1], and Yuhui Liao[2]

[1]The Fifth Affiliated Hospital of Sun Yat-sen University
[2]Dermatology Hospital of Southern Medical University
[3]Second Affiliated Hospital of Shantou University Medical College
[4]First People's Hospital of Foshan
[5]Second Affiliated Hospital of South China University of Technology
[6]Renmin Hospital of Wuhan University

May 2, 2023

Abstract

The serve burn or scald wounds always face persistent infections and self-repair function decline caused by serious tissue necrosis, leading to delayed healing or even sepsis. In this work, we proposed a click-chemistry hydrogel delivery system of antibacterial and tissue remodeling function nanovesicles for deep scald wound treatment. An hydrophilic photodynamic aggregation-induced emission photosensitizer 4-(2-(5-(4-(diphenylamino)phenyl)thiophen-2-yl)vinyl)-1-(2-hydroxyethyl) pyridin-1-ium bromide (THB) was firstly encapsulated into nanovesicles derived from easily accessible adipose stem cells (ANVs) to create THB@ANVs, which exhibits enhanced bacteria-targeting property and multiple tissue remodeling effects. To deliver THB@ANVs, an injectable click-chemistry hydrogel of carboxymethyl chitosan was used to form a wound treatment system for deep scald wounds. The hydrogel can well matching the wound morphology and respond to the acidic microenvironment of the wound to accelerate sustained release. In vivo wound healing evaluations show that the composite hydrogel can efficiently accelerate wound healing by reducing the number of bacteria, promoting early angiogenesis, and regulating immune reaction. This study provides a simple, low-cost, and effective "one-stop" strategy with diverse functions and wide applicability for scald wound remodeling and antibiosis.

1. Introduction

Scald or burn injuries deep into the dermis always face obstacles during the recovery process due to both decline in repair function and persistent infection,[1-3] which can result in chronic wound healing and pose a risk of sepsis.[4] Various tissue engineered materials with beneficial healing ingredients have been developed for serve scald or burn wound healing,[5] however, always can't realize mass production.[6] Stem cells can be expanded *in vitro* , and exhibit high activity in enhancing metabolism, regulating immunity, and promoting skin reconstruction.[7]But cell transplantation on wound is facing low survival rates, and potential safety risks on tumor cells and organ, which obstruct its clinical promotion.[8-10] While, extracellular vesicles (EVs) of stem cells not only retain their effective cytokines, but also exhibit greater safety, stability, tissue penetration, and delivery capacity.[11-13] Besides, facile nanovesicle extrusion technology from cell membranes has also been reported to replicate characteristics of EVs, making cells-derived nanovesicles a hopeful candidate for precision treatment.[14-17] However, the anti-infectious ability of nanovesicles still needs to be enhanced.

The bacteria present in the necrotic tissue invade deeply, producing toxins and other metabolites, and resulting in persistent inflammation.[18] Deep injuries that cover larger surface area (over 15% of the total adult body surface) carry a higher risk of cytokines diffusing throughout the body, which can lead to systemic inflammatory response syndrome (SIRS), multiple organ dysfunction syndrome (MODS), sepsis, and even death.[19] Besides, antibiotic resistance can easily occur due to the use of systemic antibiotics for the treatment of localized infections.[20] Photodynamic therapy without leading to drug resistance has attracted considerable attention in the field of antibiotics.[21,22] Tang et al have reported a series of aggregation-induced emission (AIE) photosensitizers that hold potential applications in bioimaging and photodynamic therapy. The aggregates of AIEgens in aqueous condition demonstrate not only high luminescence efficiencies but also efficient reactive oxygen species (ROS) generation, photostability and bacterial targeting ability.[23,24] Thus, it might be feasible to enhance the anti-infectious property of nanovesicles through AIEgens encapsulation.

For long-term wound treatment processes, continuous delivery of nanovesicles is also crucial. The commonly used injection method would result in rapid metabolism and degradation of nanovesicles on wounds, shortening their effective time.[25] To achieve sustained and effective concentration, a controllable release carrier that can protect the nanovesicles and form a reservoir on the wound is urgently needed. Based on the wet healing theory, hydrogel wound dressing can protect the wound from exposure to infections, absorb excess exudate, and promote the dissolution and exfoliation of deep necrotic tissue.[26,27] However, the preparation of controllable release hydrogels commonly requires UV light, heating or catalyst for gelation, which might harm the beneficial biological components of nanovesicles.[28] Temperature sensitive hydrogel PF-127 have been utilized for *in situ* gelation on wounds without affecting the functions of nanovesicles,[29] but it is more suitable for a constant temperature internal environment rather than on the surface of the skin.

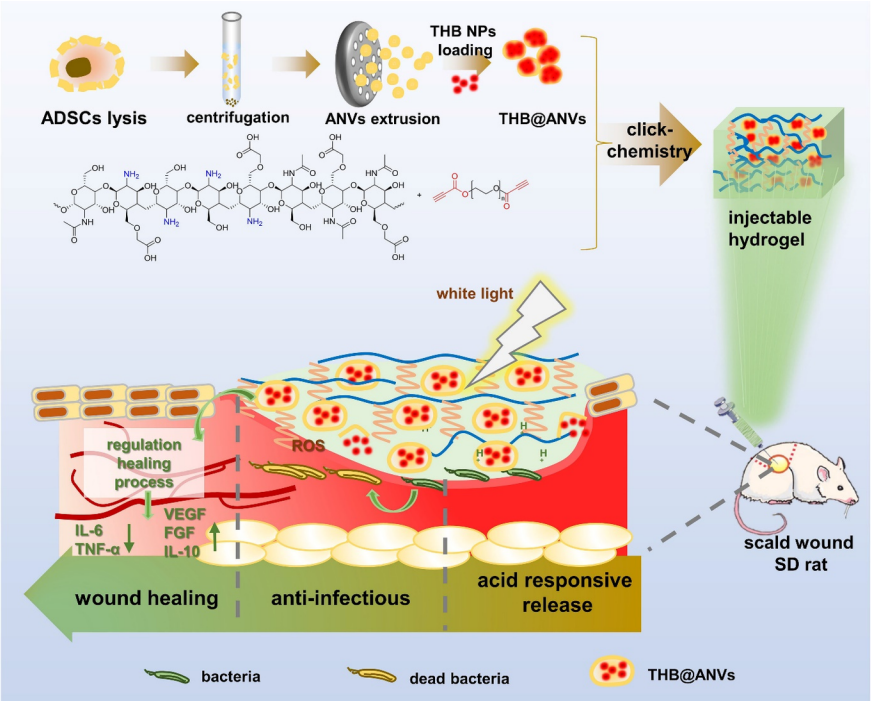

Scheme 1. Schematic illustration for the contrustion and deep scald wound repairment mechanism of THB@ANVs encapsulated hydrogel, the wound recovery process was presented from left to right.

In this study, we used easily accessible adult adipose-derived stem cells to extrude mass-produced nanovesicles (ANVs), which were then combined with photodynamic AIE nanoparticles of 4-(2-(5-(4-(diphenylamino)phenyl)thiophen-2-yl)vinyl)-1-(2-hydroxyethyl) pyridin-1-ium bromide (THB) to enhance

their anti-infectious ability (denoted as THB@ANVs). To encapsulate the THB@ANVs without altering their active ingredients, we used a heat-, light-, and catalyst-free crosslinking amino-yne click chemistry CMC-DA hydrogel composed from amino-rich water-soluble carboxymethyl chitosan (CMC) and di-activated alkyne-modified polyethylene glycol (PEG-DA)[30](Scheme 1). Our research demonstrated that this hydrogel can match the shape of a wound through injection, and that the β -aminoacrylate bond in the hydrogel can accelerate the release of contents in response to the acidic environment of the wound. *In vivo* wound healing evaluations are also conducted to investigate the effectiveness of this comprehensive hydrogel for treating bacterial infections, promoting wound tissue repair, and reducing treatment time.

2. Results and Discussion

2.1 Preparation and characterization of ANVs

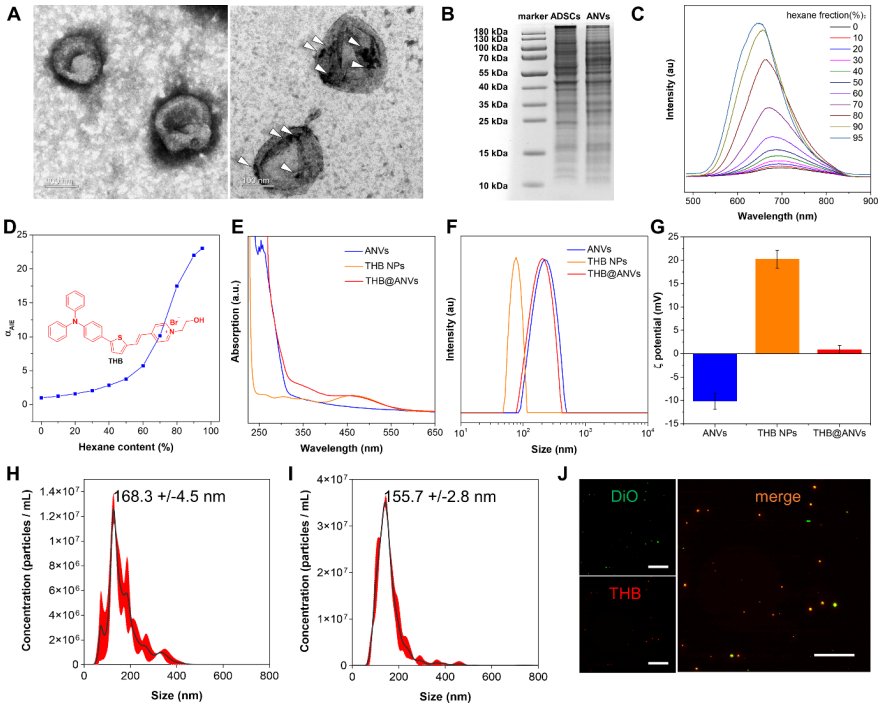

Figure 1. Characterization of ANVs and THB@ANVs: (A) The morphology of ANVs (left) and THB@ANVs (right), THB NPs in THB@ANVs were marked out by triangle. Scale bar: 100 nm. (B) Coomassie blue–stained SDS polyacrylamide gel after separation of 10 μg of total ADSCs cell lysates or ANVs. (C) PL spectra of TPAH in the mixed solution of ethanol/hexane with different hexane fractions. (D) Plots of the relative emission intensity ($\alpha_{AIE}=I\ /I_0$) versus hexane fraction. I_0 and I are the peak values of fluorescence intensities of THB in ethanol and ethanol/hexane mixtures, respectively. (E) Normalized absorption UV/vis spectra for ANVs, THB NPs, and THB@ANVs in PBS. (F) Hydrodynamic diameters and (G) Zeta potential values for ANVs, THB NPs, and THB@ANVs measured by DLS. Diameters of lidluted (H) ANVs and (I) THB@ANVs were tested by NTA. (J) DiO (green) and THB (red) co-localization within ANVs was assessed by confocal microscopy. Scale bar=100 μm.

The healing and regeneration of skin wounds is a complex physiological process that requires multiple tissues and cells to work together synergistically in order to replace, repair, and reconstruct missing tissue layers and cellular structures. Achieving this using a single pharmaceutical component can be difficult, but the components found in stem cells may fully meet this demand. Adipose-derived stem cells (ADSCs), which can be easily obtained from adipose tissues, have been shown to exert protective effects in several diseases

through the exosomes they release.[31] Therefore, we chose ADSCs as our material source for preparing ANVs using a simple extrusion method, with the aim of mimicking the functions of ADSC exosomes.[16] As shown in Figure 1A (left), ANVs display a tea cup holder-like structure with a size of 100-200 nm, as observed by transmission electron microscopy (TEM). This structure is similar to that of natural exosomes, indicating that the preparation of ANVs was successful. The nanoparticle tracking analysis (NTA) in Figure 2I shows that the size of ANVs is 168.3±4.5 nm, with a yield of $1.99 \times 10^{10}/10^6$ cells. Additionally, using the BCA detection method, the protein concentration of nanovesicles is approximately 201 μ g/10^{10}. In Figure 1B, the protein profiles of ANVs match closely with the total proteins found within whole cells, suggesting that characteristic proteins derived from ADSCs are well-retained in ANVs.

2.2 Preparation and characterization of THB@ANVs

2.2.1 Characterization of4-(2-(5-(4-(diphenylamino)phenyl)thiophen-2-yl)vinyl)-1-(2-hydroxyethyl) pyridin-1-ium bromide (THB)

Pyridinium moiety-containing red light AIEgens with π-conjugation structures have been shown to exhibit a distinct enhancement of ROS generation capacity induced by aggregation, making them a promising option for photodynamic antibacterial applications.[32] These positively charged AIEgens require only natural sunlight or white light with equivalent energy density to generate ROS [33,34]. Here, we designed a hydroxypyridinium moiety containing water soluble THB, which is expected to allow for better loading into and release from nanovesicles, while achieving high antibacterial activity. The THB was synthetized by facile organic reactions in high yield, and the structures of THB and intermediates were characterized by ^{1}H and ^{13}C nuclear magnetic resonance spectra and high-resolution mass spectra (HRMS) (Figure S1˜S5). As a hydrophilic molecule that can be well dispersed in water, the aqueous solution of THB is almost non-emissive. Thus, the AIE properties of THB were tested with different volume percentage of hexane as poor solvent (Figure 1C and 1D). The photoluminescent (PL) intensities gradually increase and bule-shifted with increasing fraction of hexane, due to the formation of nanoaggregates. The enhanced emissions in aggregates could be attributed to the restriction of rotor motions, which activate radiative decay process. The maximum absorption of THB is 464 nm (Figure S6), while the maximum emission in the aggregation state is located at 647 nm, indicating its red-emission property and large Stokes shift.

2.2.2 Characterization of THB@ANVs

THB@ANVs can be prepared by co-incubating THB nanoparticles (NPs) with 400 nm ANVs, followed by extruding the mixture through a 200 nm liposome membrane. The obtained THB@ANVs were compared with THB NPs and 200 nm ANVs without THB. As shown in Figure 1C, the characteristic absorption band of THB at 464 nm can be observed in the UV/Vis absorption spectra of THB@ANVs. The loaded THB NPs can be observed in the TEM morphology of THB@ANVs (Figure 1A, right, marked with triangles). Hydrodynamic particle size and Zeta potentials tested by DLS and NTA at optimal conditions before and after encapsulation were shown in Figure 1F˜1H. The hydration effect leads to a larger particle size measurement by DLS as compared to NTA. The isolated ANVs and THB@ANVs mainly match the TEM results, with diameters ranging from 30 to 300 nm. The particle sizes of THB@ANVs prepared with different initial concentrations of THB NPs were evaluated at a fixed ANVs concentrations of 100 μg/mL (Figure S7). An optimal initial concentration of 50 μM THB NPs was chosen to obtained a hydrodynamic diameter of 204.1 nm for THB@ANVs, which is close to that of ANVs (230.6 nm). When the concentration of THB NPs is further increased, they can also distribute onto the outer surface of the membranes. This might result in electrostatic attraction between ANVs, leading to an increase of hydrodynamic diameter. Calculated by the standard curve (Figures S8), a final concentration of 35 nmol THB/100 μg ANVs was obtained, corresponding to a loading capacity of approximately 19.6%. As shown in Figure 1J, the red fluorescence of THB has also been utilized to co-localized with the membrane labeled with 3,3-dioctadecyloxacarbocyanine perchlorate (DiO), further confirming the successful coupling of THB into ANVs.

2.3 *In vitro* wound repair promoting experiment of ANVs and THB@ANVs

2.3.1 Cell proliferation and migration promoting effects

ADSCs and its natural extracellular vesicles (EVs) have been reported to show positive impact in promoting wound healing.[35,36] The ANVs prepared in this work have similar components to ADSCs, so it is also possible to exhibit similar functions. Using HaCaT cells as a model cell type, cell scratch test and Transwell assay were employed to investigate the migration promoting effects of ANVs and THB@ANVs. The in vitro scratch wound model is a straightforward and reproducible approach for studying cells migration and wound closure. According to the results (Figure 2A), ANVs and THB@ANVs can significantly enhance migration of HaCaT cells from the edge of the scratch compared to the control group after 24 h. More HaCaT cells in the upper Transwell chamber were observed to pass through the membrane into the lower chamber when ANVs or THB@ANVs were added (Figure 2B), which is consistent with the results of cell scratch test.

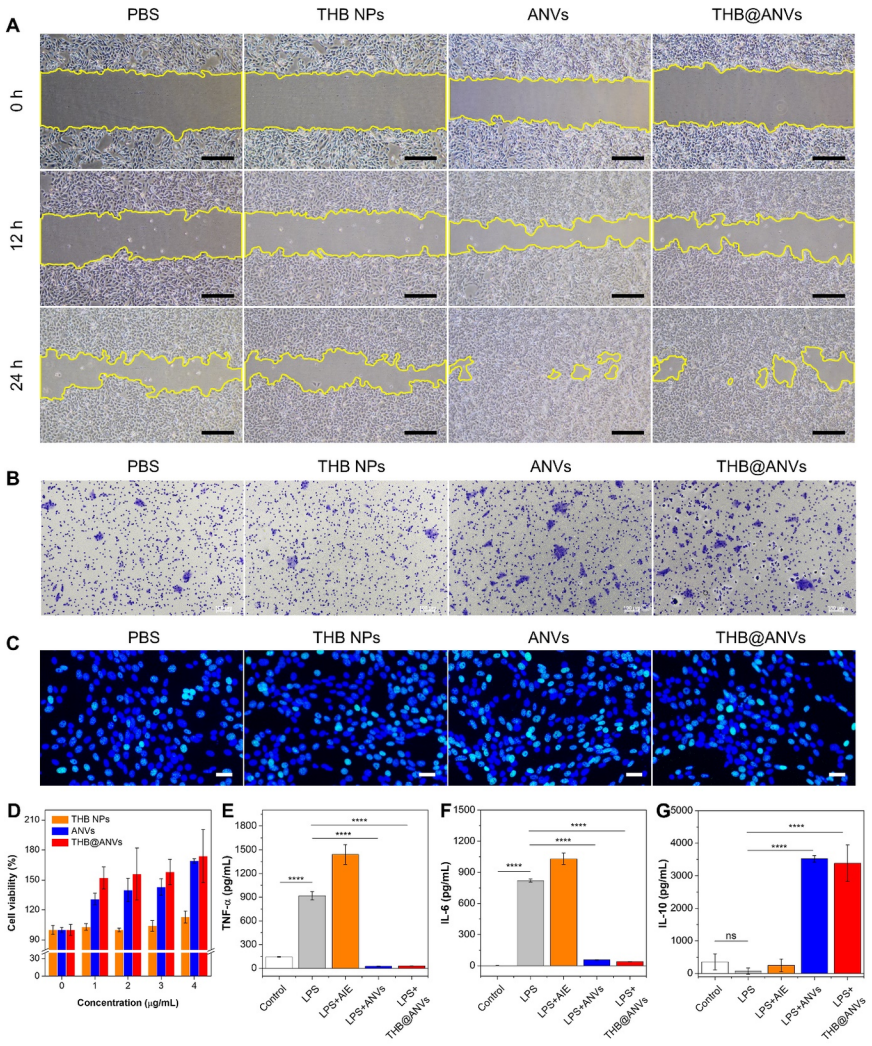

Figure 2. *In vitro* wound repair promoting experiment of THB NPs, ANVs and THB@ANVs. (A)*In vitro* wound scratch assay on HaCaT cells at 0 h, 12 h, and 24 h. Scale bar: 500 μm. (B) Effect of THB NPs, ANVs or THB@ANVs on chemotaxis of HaCaT cells by Transwell. Scale bar: 100 μm. (C) EdU incorporation assay of HaCaT cells incubated with THB NPs, ANVs or THB@ANVs. (D) Cell proliferation of THB NPs, ANVs or THB@ANVs on HaCaT cells using MTT (n = 3). Macrophages were treated with LPS (1μg/ml) and levels of (E)TNF-α, (F) IL-6, and (G)IL-10 were assessed by ELISA after incubation with THB NPs, ANVs or THB@ANVs (****, $p < 0.0001$, $n = 3$).

EdU incorporation and MTT staining assay were used to analyze their cell proliferation promoting effects. The number of EdU-positive cells increased after treatment with ANVs and THB@ANVs, indicating an increase in DNA replication levels (Figure 2C). And the number of cells in MTT also significantly increased in a dose-dependent manner (Figure 2D). Both of them prove that the ANVs and THB@ANVs still retain the function of ADSCs in promoting cell proliferation. The effect of ANVs and THB@ANVs on other types of wound repair related cells is similar, which were detailed in Figure S9 and S10. No statistical difference was observed between ANVs group and THB@ANVs group, indicating that the addition of AIE molecules did not adversely affect the proliferation and migration of cells.

2.3.2 Inflammatory regulation ability

Macrophages are innate immune cells that play a key role in host defense, wound healing, and immune regulation.[37]In the early stages of wound, M1 can cause inflammation and resist infection. However, after wound antibacterial procedure, it is necessary for macrophages to transition from M1 type to M2 type as soon as possible in order to more effectively promote the process of wound repair. ADSCs have been proven to promote wound repair and regulate inflammation.[38,39] Therefore, ANVs derived from ADSCs are expected to have the ability to regulate inflammation as well. To test this hypothesis, we used the lipopolysaccharide (LPS)-induced M1 phenotype as a positive control, while inactivated M_0 as a negative control. As shown in Figure 2E˜2G, macrophages incubated with the ANVs or THB@ANVs expressed a significant inhibition of pro-inflammatory factors (TNF-α, IL-6) and promotion of anti-inflammatory factors (IL-10). Taken together, the massively produced functionalized THB@ANVs can preserving the wound healing effect of original stem cells, and the cells exhibit little mutual repulsion towards ANVs from different individuals, enabling this kind of nanovesicles to have broad applications.

2.4 Preparation and characterization of hydrogel

2.4.1 Preparation of CMC-DA hydrogels

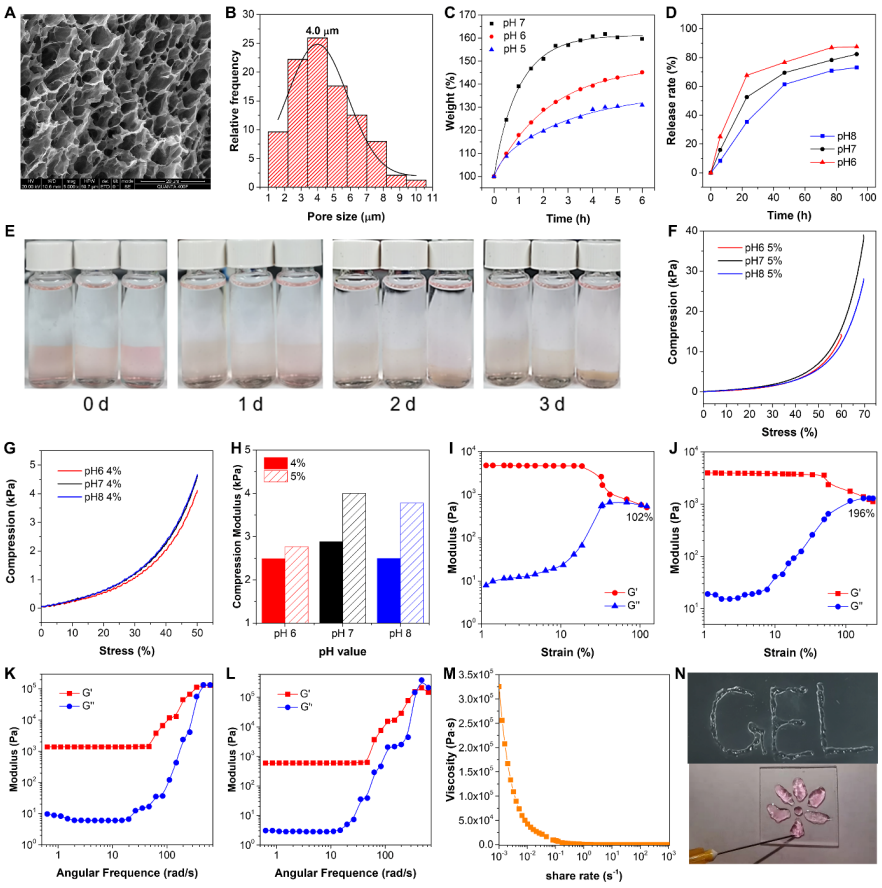

Figure 3. Characterization of CMC-DA hydrogel. (A) SEM morphology of the 4% hydrogels (Scale bar: 20 μm) and (B) statistical results of hydrogel pore size. (C) Swelling property of hydrogels in different buffer with pH of 7, 6 and 5 respectively. (D) Hydrogels in different buffer with pH of 8, 7 and 6 in 3 days, and the (E) representative images, the pH is 8, 7 and 6 from left to right, rhodamine B staining was applied to the hydrogel to enhance contrast. Stress–strain curves of 5% (F) and 4% (G) hydrogels in pH of 8, 7 and 6. (H) The Young's modulus of 5% and 4% hydrogels in pH of 8, 7 and 6. Strain sweep of (I) 5% and (J) 4% hydrogels under an angular frequency of 1 Hz, the crossover of storage modulus (G') and loss modulus (G") indicates the breakage strain. Frequency-sweep curves of the (K) 5% and (L) 4% hydrogels at a fixing strain of 3%. (M) Evolution of 4% hydrogel viscosity with shear rate. (N) The injectability and the appearance of the 4% hydrogel.

Through early research of click chemistry based on activated alkynes and amines, it was found that an amino groups containing long-chain polymer can spontaneously react with ester-actived alkyne-modified linkers to form a cross-linked network structure. [40.41]When water molecules are tightly interlocked within the cross-linked network structure, the hydrogel can be formed. Commercially accessible and water-soluble CMC contains abundant amino groups, as well as good bacteriostatic, coagulative, biocompatible and biodegradable characteristics.[42] In this work, we prepared and characterized a di-actived alkyne modified PEG-4000 cross-linking agent (PEG-DA) (Figure S11), which was utilized for a catalytic free hydrogel (CMC-DA) preparation with CMC at room temperature.

The micromorphology of the CMC-DA hydrogel was observed by scanning electron microscope (SEM) (Figure 3A). The hydrogel exhibits a uniform pore size distribution, as shown in Figure 3B, with an average diameter of approximately 4.0 μm. The high porosity percentage and interconnected pores of hydrogel pro-

vide sufficient space for loading nanovesicles and facilitate nutrient transport. The successful preparation of the hydrogel can also be confirmed by the Fourier transform infrared (FT-IR) spectrum (Figure S12). According to the test with a concentration of 1.5%˜5% and a ratio of activated alkyne and amine groups at 1:1 (Table S1), gelation can proceed smoothly when the concentration exceeds 3%. The increase in concentration promoted the speed of gelation and mechanical strength.

2.4.2 pH responsive swelling and degradation of hydrogel

Due to the presence of dynamic β -aminoacrylate bond, which can breaks in response to changes in pH[43], we tested the pH responsive swelling and degradation properties of hydrogel. Hydrogels with hydrophilic nature are able to absorb water or exudate from the wound tissue and regulate the humidity of the wound surface. As shown in Figure 3C, the swelling kinetics increased and reached the plateau after 6 h. The swelling capacity decreased as pH decrease in acidic environment, due to the occurrence of degradation. The swelling ratio of the hydrogel is also an important parameter to control the release kinetics of the drug. It is closely related to the diffusion of the drug into the surrounding media by regulating the rate of drug penetration and drug diffusion/dissolution within the hydrogel. Based on the results shown in Figure 3D, the release ratio of THB@ANVs was evaluated in alkaline, neutral, and acidic environments. There was no indication of a burst release during this period, and over 80% of the THB@ANVs can be released from hydrogel after 3 d. The release kinetics in an acidic environment were faster compared to neutral or alkaline pH, which may be related to the degradation of β -aminoacrylate bond in hydrogel under acidic conditions. It can be clearly observed in Figure 3E that the CMC-DA gel will first swell within a certain time and then degrade gradually. Thus, we hypothesis that on infected wounds with lower pH, the release of THB@ANV will be accelerated, and the hydrogel can slowly breakdown on the wound surface. By testing the release of vesicular protein from hydrogel, it can be found that hydrogel can protect the protein and keep the release process stable (Figure S13). These results proved the hydrogel a promising material for drug delivery and tissue engineering applications.

2.4.3 Mechanical behaviors and injectability of hydrogels

To achieve optimal wound repair, it is desirable to use materials with mechanical characteristics similar to the skin, which helps to maintain structural integrity when the skin tissue is deformed by external force. Considering the time cost and mechanical strength, 4% and 5% hydrogels have been chosen for exploration. We used compression stress–strain assessment to determine the mechanical characteristic of hydrogels (Figure 3F˜H). The mechanical strength of 4% and 5% hydrogels were both affected by the change of pH. Under neutral conditions, the Young's modulus of 4% and 5% hydrogel are 2.88 and 4.00 KPa, respectively, and decreased in alkaline or acidic condition. We performed strain sweep tests to determine the breakage strains of hydrogels. The corresponding elastic modulus (G') and loss modulus (G") under 1 Hz oscillation frequency are shown in Figure 3I and 3J. As the strain increased, the increase of G' and G" and a cross-over between G' and G" can be observed, indicating that the viscoelastic behavior of hydrogel shifts from an elastic gel to sol due to extreme deformation and ultimate breakage. As concentration increases, the breaking strain decreases due to a higher brittleness. The elasticity of hydrogel meets the requirements for wound repair.

Injectability is desirable in biomedical application for the localized administration of the therapeutic hydrogel. During injection, the hydrogel experiences severe share forces when passing through the narrow nozzle of a syringe or needle. Therefore, the suitable response of hydrogel to shear is essential for an applicable injectable hydrogel. To evaluate the viscoelastic properties of the hydrogels, a frequency-sweep test was conducted to measure the values of G' and G" for both hydrogels (Figure 3K, 3L). It was observed that both hydrogels exhibited a linear response range between 1˜10 Hz, affirming their elastic and stable properties. The values of G' was significantly higher than G", indicating a solid-like behavior. The frequency-sweep intersection point indicates a change of the hydrogel from solid to liquid state at high frequency. Notably, the viscosity of the 4% hydrogel decreased rapidly with an increase in shear force, indicating its possible injectability (Figure 3M). As shown in Figure 3N, the hydrogel mixture was added to a 1 mL single-channel syringe and allowed to gelation for 12 h, then injected into different pattern with a needle diameter of 16 G.

2.5 In Vitro Effects of the Hybrid Hydrogel

2.5.1 Biocompatibility

To support the growth and proliferation of cells in wound tissue, biocompatibility of hydrogel should also be tested. The biocompatibility of hydrogel was evaluated by direct live/dead staining assay and MTT assay on HaCaT cells. As shown in figure 4A and 4B, different concentrations of hydrogel had no negative effect on cellular viability and proliferation. Most cells are alive (green fluorescence) in both the control and hydrogel group, with only a few dead cells present (red fluorescence), indicating that the hydrogel have satisfactory cytocompatibility. As wound dressings inevitably come in contact with blood, hemolysis assay also was conducted to further evaluate the hemocompatibility of the hydrogels. As shown in Figure 4C, incubation of hydrogel or THB@ANVs with the red blood cells did not result in any apparent hemolysis. The results above suggest that the THB@ANVs delivered hydrogel showed good biocompatible, non-hemolytic, and suitable for wound cell growth and proliferation.

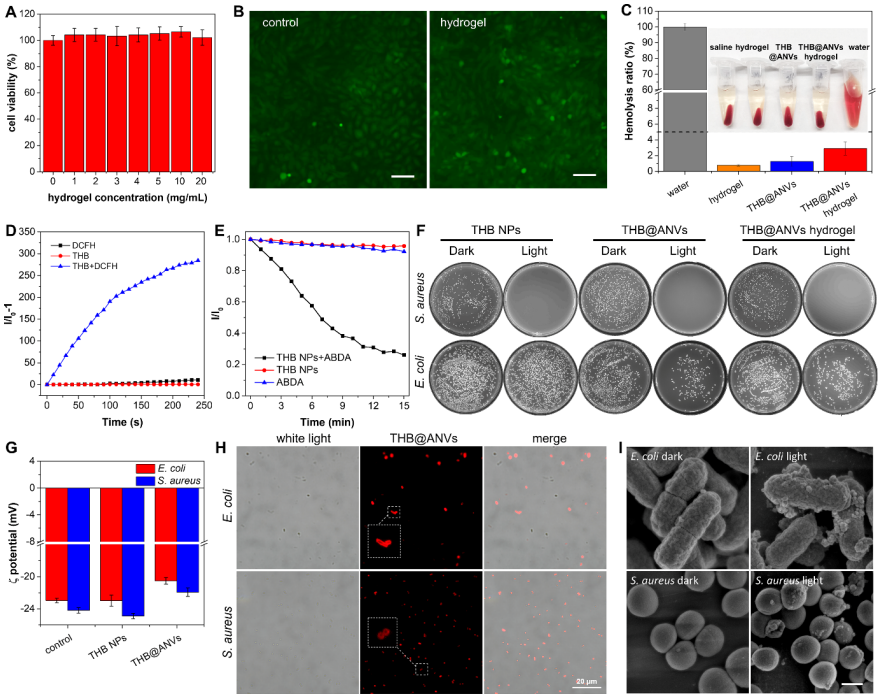

Figure 4. (A) Cell viability of HaCaT cells with different concentrations of hydrogels, n =3. (B) Cell compatibility of HaCaT cells incubated with hydrogel by live/dead staining assay, Scale bar: 100 μm. (C) Blood compatibility, and hemolysis rate of 5 mg/mL hydrogel, THB@ANVs hydrogel or corresponding quantity of THB@ANVs, n =3. Identification of ROS generation of THB NPs based on (D) DCFH and (E) ABDA indicator under 100 mW cm^{-2} white light irradiation, the concentration of THB NPs is 1 μM. Identification of $^1O_2$ generation of THB NPs based on indicator. (F) Inhibits growth of *S. aureus* and *E. coli* by THB NPs, THB@ANVs, or THB@ANVs hydrogel under 100 mW cm^{-2} white light irradiation (corresponding concentration of THB is 5 μM). (G) ζ potentials of *E. coli*and *S. aureus* pretreated with or without THB NPs or THB@ANVs, the potentials of bacteria were measured after centrifuging to the bacteria and resuspended in saline. (H) Fluorescence and merged images of*E. coli* and *S. aureus* incubated with THB@ANVs. (I) SEM images of *E.coli* and *S. aureus* treated with THB@ANVs before and after 100 mW cm^{-2} white light irradiation, Scale bar: 500nm.

2.5.2 Antibacterial ability assay

The ROS generation capability of THB was initially tested employing commercially available dichlorodihydrofluorescein diacetate (DCFH) and 9,10-anthracenediylbis(methylene)-dimalonic acid (ABDA) (Figure 4D, 4E). The fluorescence of DCFH rapidly increased with white light irradiation time at the presence of low concentration THB, demonstrating the good total ROS generation efficiency of THB. The absorbance of ABDA also decreased as the increasing generation of singlet oxygen, suggesting the potential photodynamic antibacterial performance of THB. *S. aureus* or *E. coli* was incubated with THB NPs, THB@ANVs or THB@ANVs hydrogels under the same conditions to investigate the photodynamic killing effect on Gram-negative and Gram-positive bacteria by traditional plate method. All groups exhibit high photodynamic antibacterial ability against*S. aureus* under white light irradiation with a killing rate of nearly 100 % (Figure 4F, S14). Besides, we were surprised to find that the antibacterial ability of THB against Gram-negative bacteria was notably enhanced after encapsulated into ANVs.

Both Gram-positive and Gram-negative bacteria are negatively charged, which facilitates the positively charged THB to stain, but the thick outer membranes of Gram-positive bacteria might obstruct the binding process. To figure out the reason for the increased antibacterial efficacy change of THB ANVs on Gram-positive bacteria and Gram-negative bacteria, the surface charges of the bacteria were measured by Zeta potentials (ζ), aiming to investigate the interactions between the bacteria and THB (Figure 4G). Apparent positive potential shift of both S. aureus and E. coli was observed after being incubated with THB@ANVs, while the ζ potentials of *E. coli* incubated with THB NPs remain almost constant compared with that of *E. coli* alone. The above results indicate that the ANVs encapsulation process of photosensitizers may enhanced their antibacterial activity by increasing the binding ability of THB with Gram-negative bacteria. The aggregation induced luminescence properties of THB was also used for bacteria imaging. It was visualized in Figure 4H that both the fluorescent signal of *S. aureus* and *E. coli* showing excellent image contrast to the background after incubation with THB@ANVs. This proves the bacterial targeting ability of THB@ANVs on both kind of bacteria. The higher labeling efficiency of *S. aureus* than *E. coli* can also be observed, which is consistent with the better killing effect on*S. aureus* . As shown in Figure 4I, SEM was further applied to gain insights into the morphology changes of *S. aureus* and *E. coli* upon treatment with THB@ANVs, followed by white light irradiation. After THB@ANVs-based PDT treatment, the bacteria underwent shape change of cell walls shrinkage and fusion, providing direct evidence of the bacteria killing effects.

2.6 In vivo wound healing assessment of deep second-degreescald wound

2.6.1 In vivo wound assay

Skin is the main barrier that protects the body against external damage bacterial infection. Upon scald injury, bacteria can easily penetrate during the lengthy wound recovery process. *In vitro* studies have shown that the THB@ANVs hydrogel has great promise for bacteria resist and scald wound repair. Therefore, the deep second-degree scald wound model (16mm in diameter) of rat was successfully established using a scald equipment, with parameters set at 500 g, 95 , 15s (Figure S15). As shown in Figure 5A, hydrogels were applied on the wound after debridement treatment, and *S. aureus* were dropped onto the wound surface to verify the anti-infectious ability of THB@ANVs hydrogel. Different to human, the primary wound closure of rat relies more on contracture of the loose skin, rather than re-epithelialization and deposition of connective tissue. Thus, silicone fixing rings are used to increase the tension of skins in the wound healing assessment of rats. The photographic images of the wound appearances on days 1, 3, 7, and 14 time points taken after treatment with PBS, blank hydrogels, ANVs hydrogels or THB@ANVs hydrogels on the deep second-degree scald model of rats are shown in Figure 5B. To quantitatively determine the wound regeneration, the percentages of wound sizes were measured and analyzed (figure 5C).

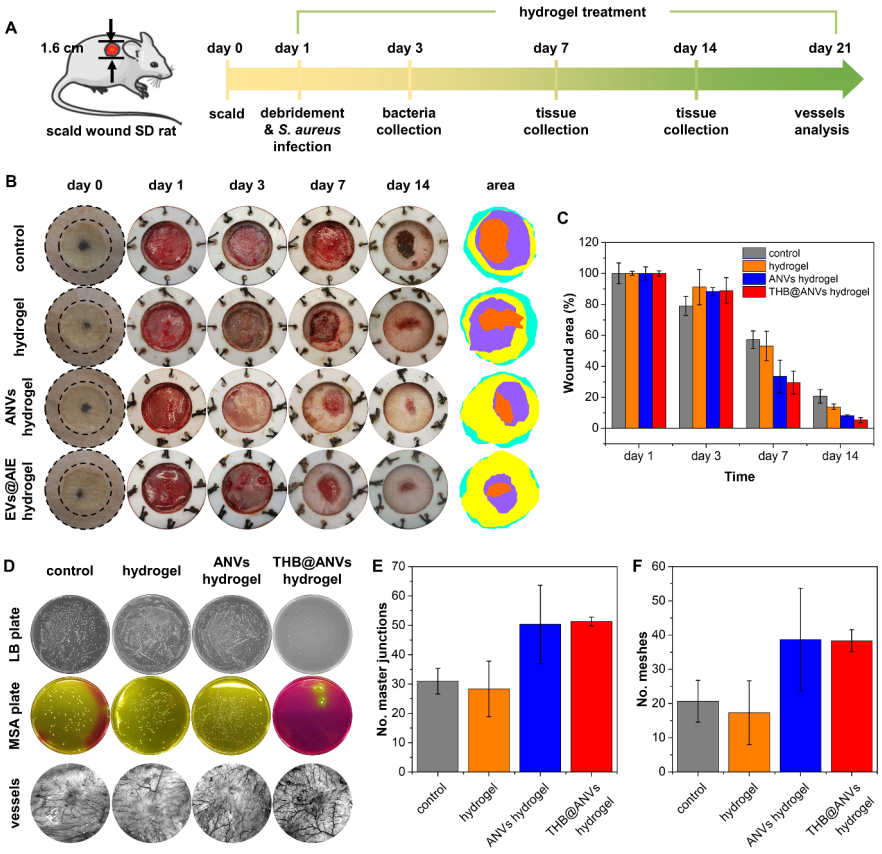

Figure 5. Evaluation of hydrogel in promoting second-degree scald wound repairment. (A) Schematic diagram of scald wound molding and the timeline of hydrogel therapeutic effect assay. (B) Representative images of the wound at day 0, 1, 3, 7, 14, and the diagrams of time-evolved wound areas. (C) Statistical analysis of the wound area ($n = 3$) (D) Photographs of bacteria from the wound tissues on day 3, cultured on Luria-Bertani (LB) medium and mannitol salt agar medium (MSA) after diluting 1000-fold, and blood vessels at the wound sites on day 21 after different treatments. Vascular regeneration analysis at the wound sites on day 21 was counted by (E) the number of master junctions and (F) the number of mashes.

The size of the wound in all groups tended to decrease, but compared with the control group and the blank hydrogel group, the wound healing speed of ANVs or THB@ANVs encapsulated hydrogels can be significantly improve. On the 3th day, due to the good antibacterial effect of THB, the bacteria infection in THB@ANVs hydrogel group were significantly inhibited, only few bacterial colonies can be obseved after white light photodynamic treatment (Figure 5D), which proved that THB@ANVs hydrogel could effectively kill and inhibit the bacteria on the wound. At the same time, it can be observed that there was already obvious granulation tissue on the wound surface of the THB@ANVs hydrogel group on 3th day. The wound area of ANVs or THB@ANVs hydrogels on the 7th and 14th day of wound healing are smaller than that of the other two groups, which proves the healing promoting ability of the ANVs. On day 21, higher vascular densities can be observed in ANVs and THB@ANVs hydrogel group with high numbers of vascular master junctions and mashes (Figure 5D˜5F). It proves that ANVs can increase the supply of nutrients to wounds by promoting angiogenesis, thereby accelerating wound healing. The above results indicate that photodynamic THB@ANVs encapsulated hydrogel is a good material to prevent bacterial infection at the defected sites and promoting wound repair at the same time.

2.6.2 Histological analysis

During the remodeling phase, collagen deposition can indicate the integrity of skin repair, with its ability to improve the tensile strength and epidermal integrity of the tissue. To further find the healing effect of the hydrogels on the wound tissues, the representative H&E and Masson's trichrome staining on days 7 and 14 were carried out on the dissected wound tissues (Figure 6A). ANVs can enhanced collagen deposition on the regenerated tissue sites. The quantified wound macroscopic observations were in accordance with the closure rates. This also confirmed the *in vitro* cell experiment results. Higher expression of collagen in scald wound area was observed in ANV hydrogel and THB@ANVs hydrogel group at day 7 and 14. Both data showed that the wounds heal of THB@ANVs hydrogel group were significantly enhanced.

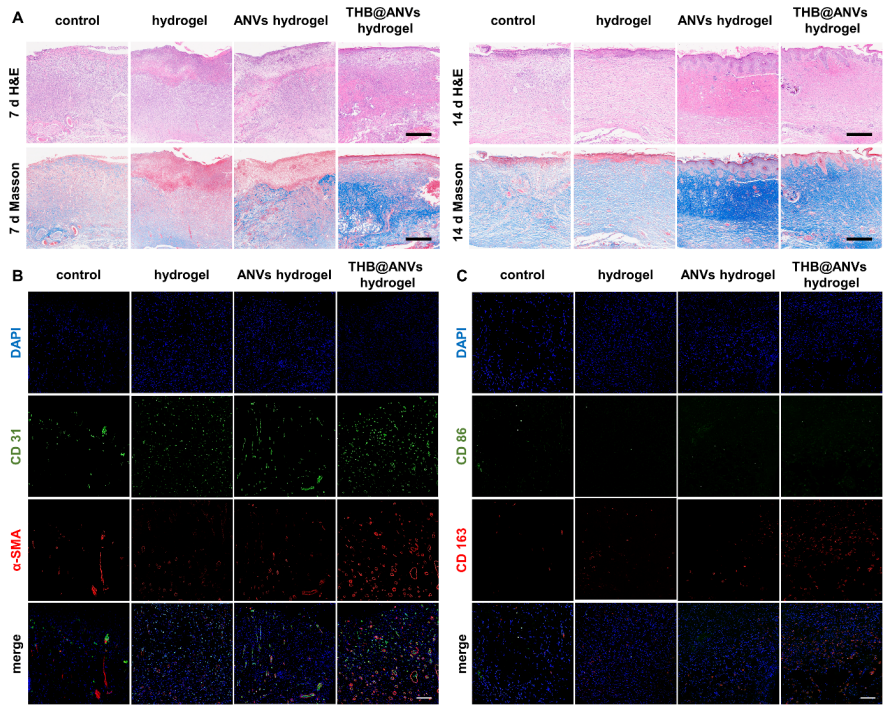

Figure 6. (A)Representative H&E-stained images and Masson's trichrome staining image of the wounds on day 7. Bar, 500 μm. Representative images of wounded (day 7) skin stained to show the expression of (B) CD31 (green) and α-SMA(red) in the wounds (blue); (C) CD86 (green) and CD163 (red) in the wounds (blue). Bar, 100 μm.

As shown in Figure 6B and 6C, to further analyze the enhancement effect in wound recovery, the immunofluorescence staining of wound tissues on day 7 were processed. In the proliferation phase, the occurrence of neovascularization is critical to ensure the transport of nutrients and oxygen to the wound site to sustain fibroblast proliferation, collagen synthesis, and re-epithelialization. Immunostaining of the platelet endothelial cell adhesion molecule-1 (CD31) can assess the presence of newly generated vessels in the granulation tissue. The α-smooth muscle actin (α-SMA) is closely related to the proliferation of fibroblasts. The wound sections from the ANVs and THB@ANVs hydrogel groups had more CD31 and α-SMA compared to the control group. This result suggests that THB@ANVs hydrogel can enhance the healing process more rapidly. Furthermore, CD86 and CD163 staining verified that the M2/M1 macrophage of THB@ANVs hydrogel group is the highest among all groups, demonstrating the wound healing had entered to proliferative phase earlier than other groups.

3. Conclusion

In conclusion, a novel AIE modified ADSCs-derived nanovesicles encapsulated in click-chemistry hydrogel has been concentrated for deep scald wound treatment and inflammation regulation. Easily accessible adi-

pose stem cells-derived nanovesicles (ANVs) are encapsulated with antibacterial photodynamic aggregation-induced emission photosensitizer (THB) to form THB@ANVs, which has been proved to show outstanding antibacterial and tissue remodeling effect. The THB@ANVs can be delivered by an injectable click-chemistry hydrogel to form a "one-stop" deep scald wound treatment system, which is worth popularizing in wound treatment. We observed the significant role of THB@ANVs hydrogel in regulating scald wound inflammation and promoting cell proliferation and migration, which is expected to achieve the prevention of wound infection sepsis, and will be further studied in our group.

Experimental section

4.1 Chemical reagents and materials

Dulbecco's Modifed Essential Medium (DMEM) and fetal bovine serum (FBS) were purchased from Gibco (Life Technologies). Phosphate buffered saline (PBS), penicillin, streptomycin, IL-10, IL-6, TNF-α ELISA kits, and DiO were purchased from Thermo Fisher Scientifc. BCA protein assay kit, calcein/PI cell viability assay kit, SDS-PAGE gel quick preparation kit, QuickBlock western, EdU cell proliferation kit (488 nm), MTT cell proliferation and cytotoxicity assay kit, crystal violet, phenylmethanesulfonyl fluoride (PMSF), ethylene diamine tetraacetic acid (EDTA), and RIPA lysis buffer were purchased from Beyotime Biotechnology. Carboxymethyl chitosan (molecular weight 240 KDa, degree of deacetylation greater than 90%, degree of amino substitution 90%) were purchased from Shanghai Macklin Biochemical Technology Co., Ltd. 3M Transparent film Dress (1624W) were purchased from 3M Tegaderm.

All the chemicals were used as received without further purification. 5-(4-(diphenylamino)phenyl)thiophene-2-carbaldehyde and 1-(2-hydroxyethyl)-4-methylpyridin-1-ium bromide were synthesized according to a literature method.

4.2 Preparation of ADSCs-derived nanovesicles (ANVs) and AIE molecular encapsulated ANVs

4.2.1 Preparation of ADSCs-derived nanovesicles (ANVs)

The Sprague-Dawley (SD) rats weighting about 100 g were used to take adipose tissue from the groin. The adipose tissue was cut into $1mm^3$ small masses and digested with 1% type I collagenase and stop by PBS after 30 min. After centrifuge at 300 xg for 10 min, the supernatant and undigested tissue were removed, precipitated cells were resuspended with DMEM containing 10% FBS. The residual red blood cells were lysed with 1×RBC lysis buffer, and the collected cells were resuspended and filtered with 200 mesh cell filter and centrifuged at 300 xg for 10 min to obtain the ADSCs. The ADSCs were purified by collecting adherent cells after amplification culture in low-sugar DMEM containing 10% FBS and and 1% (v/v) penicillin/streptomycin and used at passages 4˜5 in all experiments. The stem cell properties were identified by morphological observation and induced differentiation experiment.

The ADSCs were lysed with hypotonic cell lysis buffer (1 mmol/L $NaHCO_3$, 0.2 mmol/L EDTA, 1 mmol/L PMSF, 200 μL/10^7 cells) at 4 after cultured to 70˜80%, and then further ground with a tissue grinder. Centrifuge the solution with 3200 xg at 4 for 5 min to collect the supernatant. By repeatedly extruding the supernatant through 400 and 200 nm polycarbonate trace etching (PCTE) membrane of liposome extruder in sequence, the collected cell membrane can be reconstructed into nanovesicles (ANVs). SDS-PAGE of ADSCs and ANVs protein samples extracted by RIPA lysis buffer were further mixed with 6× loading buffer and placed at 95 *C for 10 min. Gels were running at 150 V for 30 min with SDS-PAGE rapid electrophoresis buffer.

4.2.2 Preparation of THB (4-(2-(5-(4-(diphenylamino)phenyl)thiophen-2-yl)vinyl)-1-(2-hydroxyethyl) pyridin-1-ium bromide)

THB of AIE properity was produced by simple organic reactions. The 5-(4-(diphenylamino)phenyl)thiophene-2-carbaldehyde was generated by Suzuki–Miyaura coupling reaction of 4-bromo-N,N-diphenylaniline with (5-formylthiophen-2-yl)boronic acid, and then a condensation reaction

with 1-(2-hydroxyethyl)-4-methylpyridin-1-ium bromide was underwent to give THB with a total yield of 69%.

4.2.3 Preparation of THB@ANVs

After incubated 100 μg/mL 400 nm ANVs with THB at 4 for 30 min, the THB@ANVs was then reconstructed by repeatedly extruding through a 200 nm PCTE membrane of liposome extruder. The THB@ANVs can be purified by centrifugation at 10000 xg for 30 min and then dialysis with 100 kDa ultrafiltration tube.

4.2.4 Transmission electron microscopy of ANVs and THB@ANVs

The ANVs and THB@ANVs samples were initially fixed by equal volume of 4% paraformaldehyde in PBS for 1 h, then applied to carbon Formvar film-coated transmission electron microscopy (TEM) grid, and incubated for 20 min at room temperature. After washing with PBS, the samples were fixed with 1% glutaraldehyde for 5 min, and stained with 1% uranyl acetate for 30 s, then dried before viewing.

4.3 In vitro evaluation of the repair promoting effect of ANVs and THB@ANVs

4.3.1 In vitro wound healing assay

The HaCaT cells were seeded in 24-well plates and incubated to 100% confluence. Scratches were generated using a 200 μL pipette tip. After using 500 μL PBS to wash out the non-adherent cells, 500 μL of low serum medium containing 1% FBS and ANVs or AIE@ANVs was added into each well. Images were acquired by microscope at 0 h, 12 h, and 24 h. The wound areas were measured using Image J.

4.3.2 Transwell cell migration assay

The Transwell migration assay were conducted using 24-well Transwell insert with 8 μm pore (Corning, Milan, Italy), 200 μl cell suspension (1 x 10^6 cells/ml in basic medium) was added on top of the filter membrane and incubated for 10 minutes at 37 °C and 5% CO_2 to allow the cells to settle down. Carefully added 600μl medium containing 5% FBS and ANVs or THB@ANVs into the bottom of the lower chamber without generating bubbles, and incubated for 12˜48h. After removing the media and remaining cells on top of the filter membrane, the cells on the other side of the membrane were fixed with 4% polyformaldehyde for 20 min, and then stained by 0.2% crystal violet for 5-10 minutes. Images of cells were acquired by microscope and analyzed by Image J.

4.3.3 EdU incorporation assay

EdU incorporation assay were performed using BeyoClick EdU Cell Proliferation Kit with Alexa Fluor 488 (Beyotime). Cells (4×10^4 cells/mL) in 24-well were treated with ANVs or AIE@ANVs for 24 hours, then incubated with EdU (20 mmol/L) for 2 hours. The cells were fixed with 4% paraformaldehyde for 20 minutes at room temperature, and washed with PBS (containing 3% BSA). Then, the cells were treated with Triton X-100 (0.3% in PBS) for 10 min. After washing again with PBS, the cells were incubated with 100μl click additive solution (containing $CuSO_4$ and Azide 488) at room temperature for 30 min. Nucleus was stained by 1× Hochest 33342 at room temperature for 10 min. After washing with PBS, the cells were observed by fluorescence microscopy.

4.4 Preparation and characterization of CMC-PEG hydrogel

4.4.1 Preparation of CMC-PEG hydrogel

PEG-DA was prepared in large quantities by the esterification reaction of PEG-4000 and propionic acid under the catalysis of*p* -toluenesulfonic acid in toluene according to the literature.[30] After purification, PEG-DA and CMC of equal molar ratio of functional groups were dissolved in the PBS solution of ANVs or THB@ANVs with a weight percent of 4%, the solution was stored at 4 overnight to gelation.

4.4.2 Acid responsive assay of hydrogel

Swelling: A certain weight of hydrogel was immersed in excess pH 5, 6, or 7 phosphate saline buffer. The weight was measured at predetermined time intervals after dried the surface of hydrogel. The swelling ratio was calculated as: Swelling ratio= $(W_{hydrogel}- W_0)/W_0$, where $W_{hydrogel}$is the weight after swelling and W_0 is the weight before swelling.

Release: The hydrogel samples of certain weight were put in the pH 6, 7, 8 sterilized phosphate-buffered saline (PBS) at 37 degC, which was shaken at 100 rpm/min. The samples were taken out in the time points to test the corresponding absorption of THB@ANVs. The degradation of hydrogel at different pH was also photographed.

4.4.3 MTT cell proliferation assay of hydrogel

To evaluation the biocompatibility of the hydrogels, the extraction solutions of THB@ANVs hydrogels were first prepared according to ISO 10 993–5 standard. Briefly, the hydrogel (surface area 1 cm2) was soaked in 1 ml DMEM and then placed at 37 *C for 24h to obtain the extraction solutions of the hydrogels. Afterward, 10^6 cells were cultured in the extraction solutions in 96-well plates for 24 h at 37 *C and 5% CO_2. Then, the medium was replaced with an MTT solution (0.5 mg ml^{-1}) and the plates were placed in an incubator incubated for 4 h. The precipitated formazan was dissolved in isopropanol for 15 min and the absorbance was read at 570 nm.

4.4.4 Apoptosis analysis

The number of apoptotic and necrotic cells was analyzed by AM&PI staining apoptosis detection kit. In brief, 2 x 10^5HaCaT cells were cultured overnight in 6-well plates. After removing the culture medium, the cells were incubated in the extraction solution obtained by soaking the hydrogels in culture medium for 24 h. The cells were stained with AM (5 μl) and PI (5 μl), left in dark for 15 min then observed by fluorescence microscopy.

4.4.5 Hemolysis test

The porcine red blood cells separated from the whole blood were gently wash with 3 volumes of saline, then centrifuged at 500 1000 r/min for 5 minutes, repeating the process 2˜3 times. After being diluted 20 times, the red blood cells were incubated with an equal volume of saline, deionized water, AIE EVs solution or hydrogels immersed solutions at 37 for 3h. The supernatants were obtained by centrifugating the mixture at 750g for 5min, and their absorbance at 545 nm will be measured. The hemolysis rates are calculated as the following formula: Hemolysis rate (%) = $(A-A_{saline}) / (A_{water} - A_{saline}) \times 100\%$. The hemolysis rate exceeds 5% is considered hemolysis.

4.4.6 Antibacterial ability assay of THB@ANVs

The bacteria imaging was carried by mixing 90 μL of bacteria with 10 μL newly prepared THB@ANVs for 20 min at ambient temperature, then observed on glass slides. The images were collected under FL microscope (100×, excitation filter 528-553nm, dichroic mirror 565nm, emission filter 578-663nm). Scanning electron microscopy (SEM) was applied to observe the morphologies of the bacteria before and after treated with THB@ANVs. After the treatment above, the bacteria were fixed with 2% glutaraldehyde at 4 degC overnight and then rinsed with water, followed by dehydration with a sequential ethanol/water mixtures with an increasing ethanol volume of 30%, 50%, 70%, 80%, 90%, 95%, and 100%, respectively. Finally, the samples were dropped on a silicon wafer, vacuum dried, and coated with platinum before observation.

4.4.7 Antibacterial experiment of hydrogel

The 2 cm^2 sterile hydrogels were soaked in 180 μL sterilized PBS for 3d, then 20 μL bacterial suspension (1×10^7) was added to incubation with each hydrogel for 30 min. The mixtures were irradiated with white light at a power density of 100 mW/cm^2 for 10 min. They were then diluted 10 times with saline and vigorously mixed in a centrifuge tube. Next, further diluted the mixture by a 1:100 ratio, and take 100 ul of the resulting solution to spread on Luria-Bertani agar plates. The plates were kept at 37 °C for 14˜18 h

in an incubator, followed by photography and cell counting. The tests were repeated three times for each group, and the results were expressed as killing rate (%):

Killing rate (%) = (Cell count of control-Cell count with hydrogel)/Cell count of control×100%

4.5 In vivo wound healing assessment in a deep IIdeg scald wound molding

On 0 d, The SD rats weighing 180-200 g were anesthetized with inhaled gas anesthesia (O_2 2 L/min,2% isoflurane) before surgery, and the hair on their back was shaved. To induce a deep IIdeg scald wound, a preheated copper-block (500g) of a temperature control scald instrument at the temperature of 95 degC for 15 s at the dorsal area of each rat. Twelve rats were randomly divided into four groups with different treatments: (1) Control group in which saline alone was applied to the wounds, (2) blank hydrogel group, (3) ANVs hydrogel group, (4) THB@ANVs hydrogel group. 2mm hydrogel in with the same area as the wound were applied to cover the wounds of group (2)(3)(4).

On 1d, 60 μL of 10^6 *S. aureus* were dropped onto the wound surface after debridement, then saline or hydrogel were applied to the scald wound and covered by Tegaderm film dressing (3M Deutschland GmbH, Neuss, Germany). After incubating the hydrogel on the wound for 6 hours, photodynamic therapy was performed using 100 mW/cm^2 white light source for 10 min. The sustained release time of gel is 3 days, and the frequency of dressing change is consistent with it. Photodynamic therapy was performed every day from 1˜7d, and every other day from 8˜14d, and sampled on days 3, 7, 14 and 21 have been collected. The images of wound healing regions were recorded on days 0, 1, 3, 7, and 14. The wound areas and vascular regeneration were measured and analyzed by Image J software.

4.6 Histopathological analyses

Skin tissues were fixed with 10% formaldehyde for 48 h and then embedded in paraffin and sectioned at a thickness of 4 μm. The samples were then stained with Hematoxylin & Eosin (H&E), Masson's trichrome or immunofluorescence. They were observed by a pathology slide scanner for the general assessment of wound regeneration.

Acknowledgements

This work was supported by the National Natural Science Foundation of China (82102256, 82272276, 81972019, 82102444, 88241059), the Basic and Applied Basic Research Foundation of Guangdong Province (2023A1515012375, 2021B1515120036, 2021A1515011453, 2022A1515012160), Chinese Postdoctoral Science Foundation (2021M693638), Excellent Young Researchers Program of the 5th Affiliated Hospital of SYSU (WYYXQN-2021008), National Key Research and Development Program of China (2021YFC2302200), Natural Science Fund of Guangdong Province for Distinguished Young Scholars (2022B1515020089), Hubei Province Natural Science Foundation for Distinguished Young Scholars (2022CFA089).

Xu Chen, Meijiao Zhao, Qihu Xie and Sitong Zhou contributed equally to this work.

Conflict of Interests

The authors declare no conflict of interests.

Ethics Statement

All animal experiments of the present study were performed according to the ARVO Statement for the Use of Animals in Ophthalmic and approved by the Animal Ethics Committee of the Fifth Affiliated Hospital, Sun Yat-sen University, Zhuhai, China (2022, L399-1). All the authors listed have approved the animal study.

Supporting Information

Supporting Information is available from the Wiley Online Library or from the author.

Received: ((will be filled in by the editorial staff)) Revised: ((will be filled in by the editorial staff)) Published online: ((will be filled in by the editorial staff))

References

1. V. Pavoni, L.Gianesello, L. Paparella, L. T. Buoninsegni, E. Barboni,*Scand. J. Trauma Resus.* **2010** , *18* , 24.

2. Y. Yoshino, M. Ohtsuka, M. Kawaguchi, K. Sakai, A. Hashimoto, M. Hayashi, N. Madokoro, Y. Asano, M. Abe, T. Ishii, T. Isei, T. Ito, Y. Inoue, S. Imafuku, R. Irisawa, M. Ohtsuka, F. Ogawa, T. Kadono, T. Kawakami, R. Kukino, T. Kono, M. Kodera, M. Takahara, M. Tanioka, T. Nakanishi, Y. Nakamura, M. Hasegawa, M. Fujimoto, H. Fujiwara, T. Maekawa, K. Matsuo, O. Yamasaki, A. Le Pavoux, T. Tachibana, H. Ihn,*J. Dermatol.* **2016** , *43* , 989.

3. C. E. Salyer, C. Bomholt, N. Beckmann, C. B. Bergmann, C. A. Plattner, C. C. Caldwell, *Surg. Infect.* **2021** , *22* , 113.

4. M. P. Rowan, L. C. Cancio, E. A. Elster, D. M. Burmeister, L. F. Rose, S. Natesan, R. K. Chan, R. J. Christy, K. K. Chung, *Crit. Care* **2015** , *19* , 243.

5. L. Li, Z. Y. He, X. W. Wei, Y. Q. Wei, *Regen. Biomater.***2016** , *3* , 99.

6. P. Everts, K. Onishi, P. Jayaram, J. F. Lana, K. Mautner, *Int. J. Mol. Sci.* **2020** , *21* , 7794.

7. Z. Li, P. Maitz, *Burns Trauma* **2018** , *6* , 13.

8. A. Shpichka, D. Butnaru, E. A. Bezrukov, R. B. Sukhanov, A. Atala, V. Burdukovskii, Y. Zhang, P. Timashev, Stem Cell Res. Ther. **2019** ,*10* , 94.

9. R. Yang, F. Liu, J. Wang, X. Chen, J. Xie, K. Xiong, *Stem Cell Res. Ther.* **2019** , *10* , 229.

10. X. Sun, W. Song, L. Teng, Y. Huang, J. Liu, Y. Peng, X. Lu, J. Yuan, X. Zhao, Q. Zhao, Y. Xu, J. Shen, X. Peng, L. Ren, *Bioact. Mater.***2022** , *25* , 640.

11. S. Rani, A. E. Ryan, M. D. Griffin, T. Ritter, *Mol. Ther.***2015** , *23* , 812.

12. P. Hu, Q. Yang, Q. Wang, C. Shi, D. Wang, U. Armato, I. D. Pra, A. Chiarini, *Burns Trauma* **2019** , *7* , 38.

13. C. Liu, Y. Wang, L. Li, D. He, J. Chi, Q. Li, Y. Wu, Y. Zhao, S. Zhang, L. Wang, Z. Fan, Y. Liao. *J. Control. Release***2022** , *349* , 679.

14. P. Guo, S. Busatto, J. Huang, G. Morad, M. A. Moses, *Adv. Funct. Mater.* **2021** , *31* , 2008326.

15. H. Wu, X. Jiang, Y. Li, Y. Zhou, T. Zhang, P. Zhi, J. Gao,*Adv. Funct. Mater.* **2020** , *30* , 2006169.

16. C. Hu, T. Lei, Y. Wang, J. Cao, X. Yang, L. Qin, R. Liu, Y. Zhou, F. Tong, C. S. Umeshappa, H. Gao, *Biomaterials* **2020** ,*255* , 120159.

17. Y. Wen, Q. Fu, A. Soliwoda, S. Zhang, M. Zheng, W. Mao, Y. Wan,*J. Extracell. Vesicles* **2022** , *1* , 100004.

18. B. Li, W. Wang, L. Zhao, D. Yan, X. Li, Q. Gao, J. Zheng, S. Zhou, S. Lai, Y. Feng, J. Zhang, H. Jiang, C. Long, W. Gan, X. Chen, D. Wang, B. Z. Tang, Y. Liao, *ACS Nano* **2023** , *17* , 4601.

19. E. B. Souto, A. F. Ribeiro, M. I. Ferreira, M. C. Teixeira, A. A. M. Shimojo, J. L. Soriano, B. C. Naveros, A. Durazzo, M. Lucarini, S. B. Souto, A. Santini, *Int. J. Mol. Sci.* **2020** , *21* , 393.

20. G. Taubes, *Science* **2008** , *321* , 356.

21. J. Zhang, F. Zhou, Z. He, Y. Pan, S. Zhou, C. Yan, L. Luo, Y. Gao,*ACS Appl. Mater. Inter.* **2022** , *14* , 30533.

22. J. Zheng, X. Long, H. Chen, Z. Ji, B. Shu, R. Yue, Y. Liao, S. Ma, K. Qiao, Y. Liu, Y. Liao, *Front. Mol. Biosci.* **2022** ,*9* , 845179.

23. J. Sun, H. Li, X. Gu, B. Z. Tang, *Adv. Healthc. Mater.***2021** , *10* , e2101177.

24. D. Zhu, Y. Duo, M. Suo, Y. Zhao, L. Xia, Z. Zheng, Y. Li, B. Z. Tang, *Angew. Chem. Int. Ed. Engl.* **2020** , *59* , 13836.

25. C. Han, D. Jeong, B. Kim, W. Jo, H. Kang, S. Cho, K. H. Kim, J. Park, *ACS Biomater. Sci. Eng.* **2019** , *5* , 1534.

26. Y. Yao, A. Zhang, C. Yuan, X. Chen, Y. Liu, *Biomater. Sci.***2021** , *9* , 4523.

27. H. Zhang, M. Song, C. Hu, Z. Zhang, S. Zhang, Y. Zhang, Y. Yang, P. Zhou, L. Zheng, L. Li, M. Mao, Y. S. Zhang, P. Ji, X. Zhang. https://doi.org/10.1002/agt2.332.

28. C. Owh, V. Ow, Q. Lin, J. H. M. Wong, D. Ho, X. J. Loh, K. Xue,*Biomater. Adv.* **2022** , *141* , 213100.

29. E. Coffin, A. Grangier, G. Perrod, M. Piffoux, I. Marangon, I. Boucenna, A. Berger, L. M'Harzi, J. Assouline, T. Lecomte, A. Chipont, C. Guerin, F. Gazeau, C. Wilhelm, C. Cellier, O. Clement, A. K. A. Silva, G. Rahmi, *Nanoscale* **2021** , *13* , 14866.

30. J. Huang, X. Jiang, *ACS Appl Mater Inter.* **2018** ,*10* , 361.

31. E. Coffin, A. Grangier, G. Perrod, M. Piffoux, I. Marangon, I. Boucenna, A. Berger, L. M'Harzi, J. Assouline, T. Lecomte, A. Chipont, C. Guérin, F. Gazeau, C. Wilhelm, C. Cellier, O. Clément, A. K. A. Silva, G. Rahmi, *Nanoscale* , **2021** , *13* , 14866.

32. M. Kang, C. Zhou, S. Wu, B. Yu, Z. Zhang, N. Song, M. M. S. Lee, W. Xu, F. J. Xu, D. Wang, L. Wang, B. Z. Tang, *J. Am. Chem. Soc.***2019** , *141* , 16781.

33. Wang, D.; Su, H.; Kwok, R. T. K.; Hu, X.; Zou, H.; Luo, Q.; Lee, M. M. S.; Xu, W.; Lam, J. W. Y.; Tang, B. Z. Chem Sci 2018, 9, 3685.

34. J. Sun, Y. Bai, E. Y. Yu, G. Ding, H. Zhang, M. Duan, P. Huang, M. Zhang, H. Jin, R. T. Kwok, Y. Li, G. G. Shan, B. Z. Tang, H. Wang,*Biomaterials* **2022** , *291* , 121898.

35. C. Li, S. Wei, Q. Xu, Y. Sun, X. Ning, Z. Wang, *Stem Cell Rev. Rep.* **2022** , *18* , 952.

36. Y. An, S. Lin, X. Tan, S. Zhu, F. Nie, Y. Zhen, L. Gu, C. Zhang, B. Wang, W. Wei, D. Li, J. Wu, *Cell Prolif.* **2021** ,*54* , e12993.

37. Y. Xiong, Y. Xu, F. Zhou, Y. Hu, J. Zhao, Z. Liu, Q. Zhai, S. Qi, Z. Zhang, L. Chen, *Bioeng. Transl. Med.* **2023** , *8* , e10373.

38. H. Zhao, Q. Shang, Z. Pan, Y. Bai, Z. Li, H. Zhang, Q. Zhang, C. Guo, L. Zhang, Q. Wang, *J. Diabetes* **2018** , *67* , 235.

39. X. Bai, J. Li, L. Li, M. Liu, Y. Liu, M. Cao, K. Tao, S. Xie, D. Hu,*Front. Immunol.* **2020** , *11* , 1391.

40. B. He, J. Zhang, J. Wang, Y. Wu, A. Qin, B. Z. Tang,*Macromolecules* **2020** , *53* , 5248.

41. X. Chen, T. Bai, R. Hu, B. Song, L. Lu, J. Ling, A. Qin, B. Z. Tang,*Macromolecules* **2020** , *53* , 2516.

42. M. He, L. Shi, G. Wang, Z. Cheng, L. Han X., Zhang, C. Wang, J. Wang, P. Zhou, G. Wang, *Int. J. Biol. Macromol.* **2020** ,*155* , 1245.

43. W. Denissen, G. Rivero, R. Nicolaÿ, L. Leibler, J. M. Winne, F. E. D. Prez, *Adv. Funct. Mater.* **2015** , *25* , 2451.

The table of contents entry :

Easily accessible adipose stem cells-derived nanovesicles (ANVs) are encapsulated with antibacterial photodynamic aggregation-induced emission photosensitizer (THB) to form THB@ANVs, which has been proved

to show outstanding antibacterial and tissue remodeling effect. The THB@ANVs can be delivered by an injectable click-chemistry hydrogel to form a “one-stop” deep scald wound treatment system.

Keywords scald wound, hydrogel, nanovesicles, aggregation-induced emission, adipose stem cells

Xu Chen#, Meijiao Zhao#, Qihu Xie#, Sitong Zhou#, Yanan Qianzuo, Xiaoping Zhong, Judun Zheng, Ronghua Yang*, Xianjin Du*, Jinyu Xia*, Yuhui Liao*

Click-Chemistry Hydrogel Delivery Aggregation-Induced Emission-Active Nanovesicles Enables “One-Stop” Remodeling and Antibiosis on Deep Scald Wound

整体构思

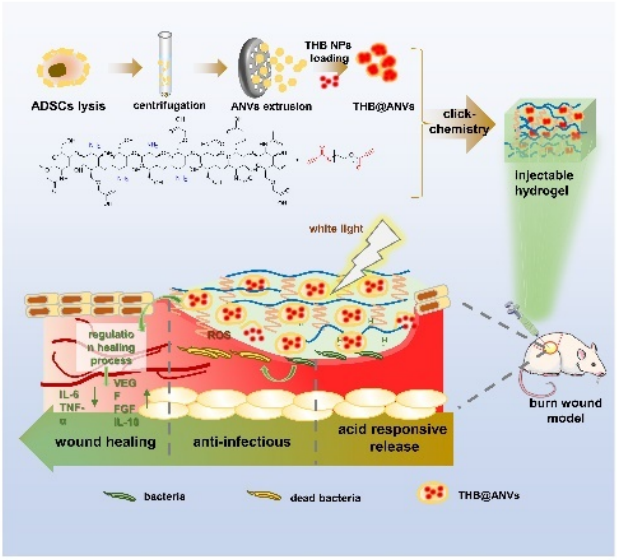

For Table of Contents Only